MOEM

Modern Electronic Materials 2024; 10(4): 251–261
DOI 10.3897/j.moem.10.4.144317

Research Article

In situ reflection electron microscopy for the surface processes analysis during sublimation and epitaxial growth of layered metal chalcogenides

Sergei A. Ponomarev[1,2], Dmitry I. Rogilo[1,2], Konstantin E. Zakhozhev[1,2], Dmitry A. Nasimov[1], Nina N. Kurus[1], Anton K. Gutakovskii[1], Konstantin A. Kokh[3], Alexander G. Milekhin[1], Dmitry V. Sheglov[1], Alexander V. Latyshev[1,2]

1 *Rzhanov Institute of Semiconductor Physics of the Siberian Branch of Russian Academy of Sciences, 13 Academician Lavrentieva Ave., Novosibirsk 630090, Russian Federation*

2 *Novosibirsk State University, 1 Pirogova Str., Novosibirsk 630090, Russian Federation*

3 *V.S. Sobolev Institute of Geology and Mineralogy of the Siberian Branch of Russian Academy of Sciences, 3 Academician Koptyuga Ave., Novosibirsk 630090, Russian Federation*

Corresponding author: Sergei A. Ponomarev (ponomarev@isp.nsc.ru)

Received 28 September 2024 ♦ **Accepted** 17 November 2024 ♦ **Published** 30 December 2024

Citation: Ponomarev SA, Rogilo DI, Zakhozhev KE, Nasimov DA, Kurus NN, Gutakovski AK, Kokh KA, Milekhin AG, Sheglov DV, Latyshev AV (2024) *In situ* reflection electron microscopy for the surface processes analysis during sublimation and epitaxial growth of layered metal chalcogenides. *Modern Electronic Materials* 10(4): 251–261. https://doi.org/10.3897/j.moem.10.4.144317

Abstract

Using *in situ* reflection electron microscopy we have presented latest studies of Si(111) and Bi_2Se_3(0001) surface processes during sublimation, homo- and heteroepitaxial growth of layered metal chalcogenides. A structural kinetic diagram of interaction between a selenium molecular beam and Si(111) surface has been demonstrated. We have shown congruent sublimation caused by annealing of Bi_2Se_3(0001) substrates in a selenium flux, visualized and described layer by layer homoepitaxial Bi_2Se_3 growth. We have presented techniques of layered $SnSe_2$ and In_2Se_3 growth on Si(111) and Bi_2Se_3(0001) surfaces and shown that heteroepitaxial growth starts with the 2D islands formation. The nucleation and growth of an impurity-induced phase in the form of 0.4 nm high 2D islands during high-temperature submonolayer indium deposition on Bi_2Se_3(0001) under exposure to Se molecular beam has been demonstrated.

Keywords

metal chalcogenides, *in situ* reflection electron microscopy, surface

1. Introduction

A new approach to graphene synthesis was suggested in the early 21st century by A.K. Geim and K.S. Novoselov [1] and favored a multifold growth of interest to studies of other 2D materials including layered metal chalcogenides [2–6]. Layered metal chalcogenides exhibit semiconducting, metallic, dielectric and topological insulator properties and therefore can be used in advanced photovoltaics, spintronics, electronics and photonics [7–12]. Along with the abovementioned properties those materials are distinguished by the formation of 1 nm thick molecular layers in which the atoms are bound by strong covalent bonds whereas the layers are

interconnected by weak Van der Waals interaction [3, 13]. The latter property delivers high flexibility of the layers and resistance to mechanical strains such as bending/flexure which allowed fabricating highly durable flexible GaSe photodetectors on mica substrates: their photovoltaic response was retained after multiple bending/flexure cycles [14]. Furthermore, the nanometer-order thickness of the layers and a Van der Waals gap between them provide a large effective area of the layered materials and therefore allows them to be used as sensing elements of gas sensors [15–17]. As a result, the demonstrated properties of layered metal chalcogenides have great potential for the different electronic and optoelectronic devices fabrication [13, 18, 19].

Molecular beam epitaxy (MBE) is a widely used technique of layered metal chalcogenides synthesis on crystalline substrate surfaces [20]. However, like other epitaxial growth techniques this one does not prevent the formation of point defects [21], twin domains [22] and other defects during growth, as well as the growth of polymorphs having similar stoichiometric composition but different crystalline structures [23, 24]. Some defects form at the heterointerface during the nucleation and growth of first layers. Therefore developing high-quality Van der Waals heterostructures growth techniques on substrates on an industrial scale requires data about early growth stages of layered metal chalcogenides, include metal and chalcogenide interaction with crystalline substrates during adsorption, islands formation and further film growth. Obtaining that information requires *in situ* characterization methods allowing real time monitoring of surface processes, such as surface structure and morphology transformations during atomic adsorption, diffusion and interaction, both mutual and with the substrate.

An informative method of studying surface processes is *in situ* reflection electron microscopy [25–30] having sufficient sensitivity to analyze the transformations of surface structure and visualize crystal surface morphology evolution in real time mode. This work presents recent *in situ* reflection electron microscopy data on Si(111) and Bi_2Se_3(0001) surface processes during metal (In, Sn) and chalcogen (Se) adsorption as well as sublimation and epitaxial growth of layered $SnSe_2$ and In_2Se_3 metal chalcogenides.

2. *In situ* reflection electron microscopy and its characteristics

In situ reflection electron microscopy (REM) has been developed on the basis of the upgraded Jem-7A transmission electron microscope [31] and is used for the *in situ* characterization of morphological transformations on crystal surfaces during sublimation (up to the substrate melting point) [30–32], homo- and heteroepitaxy [29, 30, 33], and adsorption of different materials, e.g. indium, tin and selenium [27, 28, 30, 34, 35]. *In situ* REM allows obtaining reflection high-energy electron diffraction patterns (RHEED) with electron energies of ~100 keV and visualizing electron microscopic surface imaging. An electron beam is incident onto the substrate surface at a low Bragg angle thus delivering high sensitivity to the substrate surface structure and visualizing objects like atomic steps on crystal surface [32], surface areas with different superstructural reconstruction [26, 27] and some types of defects, e.g. screw dislocations emerging on the surface [32]. Due to the low electron beam incidence angle, the spatial resolution and electron microscopic image magnification in the beam incidence direction are smaller (by ~50 times) than in the direction perpendicular to beam incidence (the vertical and horizontal scale grids in Fig. 1(*b*, *d*) have different scale units).

The test materials for the *in situ* studies were 8.0×1.1–2.5×0.3 mm sized crystal specimens cut from Si(111) wafers or exfoliated from a Bi_2Se_3(0001) single crystal with a sharp blade. Before the experiments the specimen surfaces were cleaned from oxide layers by annealing in the REM column in a differential vacuum cryopanel producing ultrahigh vacuum in the specimen location [32]. The silicon specimens were annealed at 1300 °C and the bismuth selenide specimens, at 450 °C for 10 min with simultaneous selenium deposition at a rate more than 0.1 nm/s. The specimens were heated with DC or AC current. After the experiments the specimens were rapidly cooled to room temperature, and further *in situ* studies were conducted with atomic force microscopy (AFM, Bruker multimode 8), scanning electron microscopy (SEM, Hitachi SU8220, accelerating voltage 1.5 kV), Raman scattering (Horiba XploRa Plus, spectra taken at 532 nm) and high-resolution electron microscopy (HRTEM, Titan 80-300, FEI, accelerating voltage 300 kV).

3. Si(111) surface interaction with Se molecular beam

For the formation of a Van der Waals bond at the film/substrate interface the dangling Si(111) bonds are passivated with chalcogenide atoms before growing layered metal chalcogenides [36, 37]. Although the interaction between selenium atoms and silicon surface was studied and surface etching due to the formation and desorption of $SiSe_2$ molecules was demonstrated in the works [36, 38, 39], the kinetics of Si(111) surface etching depending on selenium flux and specimen temperature has remained unclear.

The interaction between selenium molecular flux and Si(111) surface in the 600–1300 °C range at different molecular selenium flux intensities was experimentally studied using *in situ* REM earlier [25, 26, 34]. Detailed analysis of the data allowed identifying and separating three kinetic modes of silicon surface

etching with selenium beams; those kinetic modes are schematically shown in a structural kinetic diagram (Fig. 1*a*). At low temperatures (below 600 °C in Fig. 1*a*) the etching kinetics is restricted by the formation and desorption of $SiSe_2$ molecules with the activation energy 2.65 eV. At below 830 °C the atomically-clean Si(111) surface has a 7×7 surface reconstruction (superstructure) the lattice parameter of which is 7 times greater than Si(111)–1×1 [40]. At below 600 °C (the grey area below the T_1 line) etching occurs at a low rate (<0.001 ML/s, where 1 ML = $7.8 \cdot 10^{14}$ cm^{-2}), the 7×7 superstructure on the surface is destroyed and an impurity-induced disordered 1×1–Se surface structure (phase) with a Se atomic concentration of 1/2 ML is formed [36]. At above 600 °C (the dark-grey area above the T_1 line) the etching rate is restricted by the selenium molecular flux incident onto the surface. It was simultaneously shown that in the 600–830°C range etching is accompanied by the formation, growth and coalescence of 2D vacancy islands (Fig. 1(*b*, *c*)), whereas at above 830 °C (the white area) the Si(111) surface is etched due to the flow of atomic steps (Fig. 1(*d*, *e*)). At high temperatures (~1150 °C, above the T_2 line) sublimation starts to dominate in the overall silicon flow from the surface, also accompanied by the motion of atomic steps.

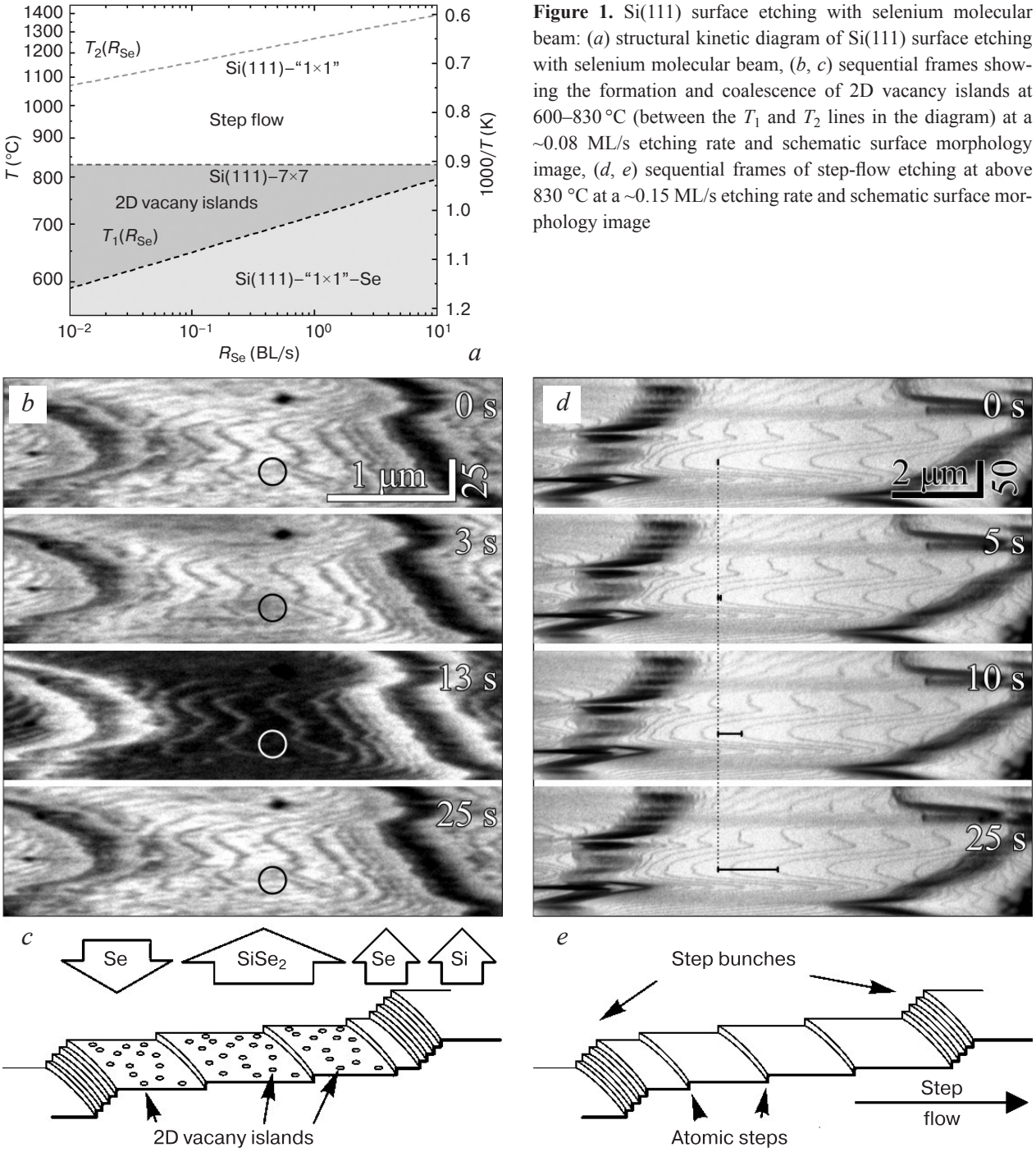

Figure 1. Si(111) surface etching with selenium molecular beam: (*a*) structural kinetic diagram of Si(111) surface etching with selenium molecular beam, (*b*, *c*) sequential frames showing the formation and coalescence of 2D vacancy islands at 600–830 °C (between the T_1 and T_2 lines in the diagram) at a ~0.08 ML/s etching rate and schematic surface morphology image, (*d*, *e*) sequential frames of step-flow etching at above 830 °C at a ~0.15 ML/s etching rate and schematic surface morphology image

4. Growth of layered $SnSe_2$ and In_2Se_3 on Si(111) surface

Dangling bond passivation on Si(111) surface with selenium atoms [36, 37] is a necessary condition of substrate preparation for Van der Waals epitaxy. Si(111) surface preparation was started with petroleum ether cleaning and annealing in the *in situ* REM column at 1300 °C for 600 s followed by cooling to 450 °C [33]. Cooling caused a transition from the disordered 1×1 surface phase to the 7×7 superstructure at 830 °C showing itself in the respective transformation of the RHEED pattern [33]. Then the Se and Sn (or In) fluxes were calibrated at about 450 °C by the time of 7×7 superstructure reflection attenuation in the RHEED patterns. Selenium forms an impurity-induced 1×1-Se phase with 1/2 ML coverage whereas indium and tin form √3×√3 surface phases with 1/3 ML coverage. The In/Se and Sn/Se flux ratios were chosen to be between 1/20 and 1/10 since selenium excess stabilizes the stoichiometry of the growing $SnSe_2$ and In_2Se_3 films [41, 42]. After evaporator calibration the substrate surface was prepared for growth. The latter stage included (1) surface annealing at 1250 °C; (2) deposition of 1/3 ML indium at 450 °C; (3) short 600 °C anneal for indium atom removal from the surface (the 7×7 reconstruction has not sufficient time to form); (4) surface passivation with selenium atoms at 100 °C [29]. Then about one molecular layer of $SnSe_2$ (~0.6 nm thickness) or In_2Se_3 (~1.0 nm thickness) was deposited, followed by rapid heating to the growth temperatures causing amorphous layer crystallization. The growth continued until the emergence of RHEED pattern reflections typical of 3D island formation (Fig. 2). Then the as-grown films were studied using *ex situ* AFM, Raman scattering, HRTEM and SEM methods.

Figure 3(*a*, *b*) shows AFM images of ~50 nm thick $SnSe_2$ film surface. The film surface morphology images show 0.6 nm high layered islands the height of which is in agreement with that of the $SnSe_2$ layers [43]. The $SnSe_2$ film surface has two sets of terrace-shaped hills with weakly triangular facets oriented mirror-wise to one another. This indicates the presence of a predominant orientation (epitaxiality) of film domains relative to the substrate and the formation of twin defects in the film. One can also see screw-component dislocation emergence on the surface in a concentration of ~18 μm^{-2}. The white areas in the AFM image are 3D SnSe islands forming at late experiment stages as follows from the RHEED patterns. Analysis of the Raman spectra (Fig. 3*c*) revealed a set of oscillation modes corresponding to layered bulk $SnSe_2$. The E_g (118 cm^{-1}) and A_{1g} (185 cm^{-1}) modes correspond to oscillations within and beyond the layer plane, in agreement with earlier data for the 1T-$SnSe_2$ phase (119.3 cm^{-1} and 186.7 cm^{-1}) [44]. The additional peak at a 10^7 cm^{-2} corresponds to the B_{3g} oscillation mode of the SnSe phase [45] which was synthesized on the $SnSe_2$ film surface in the form of 3D islands at a late growth stage due to a decrease in the selenium flux. Figure 3(*d–f*) shows the HRTEM images of the film where one can see $SnSe_2$ layers (Area 1) underlying SnSe layers (Area 2) covered with a residual disordered epoxy resin layer which remained after specimen preparation for HRTEM study [29]. HRTEM analysis suggests that $SnSe_2$ has a $P\bar{3}m1$ (No. 164) hexagonal lattice with the parameters $a = 0.38$ nm and $c = 0.62$ nm, the basal plane being (001), parallel to the (111) plane of silicon [29, 33]. Thus *ex situ* AFM, HRTEM and Raman scattering data suggest that layered 1T-$SnSe_2$ growth has a predominant orientation relative to the substrate and occurs by a 2D island mechanism transiting to 3D SnSe island growth with a decrease in the selenium flux.

Figure 4(*a*, *b*) shows an example of ~20 nm thick In_2Se_3 film morphology grown without preliminary passivation where one can see disordered layered islands without clear facets, 1–3 μm in lateral dimensions and 10–15 nm in height. The tops of the islands are in the form of atomically smooth terraces divided by ~1 nm high molecular steps which is in agreement with the height of an In_2Se_3 molecular layer, the concentration of screw dislocations being ~2 μm^{-2}. The Raman spectra shown in Fig. 4*c* exhibit a set of oscillation modes at 110, 176 and 205 cm^{-1} corresponding to the β-In_2Se_3 phase [23, 46]. In_2Se_3 growth experiments with preliminary Si(111) surface passivation by selenium atoms [47] reported the formation of 2D islands with clear facets but without any orientation relative to the substrate. Thus, comparing the surface morphology between the $SnSe_2$ and In_2Se_3 films grown on passivated and non-passivated Si(111) surfaces one can see that surface passivation provides primarily the faceting of the 2D islands and, given optimum growth parameters at early stages, clear orientation relative to the substrate.

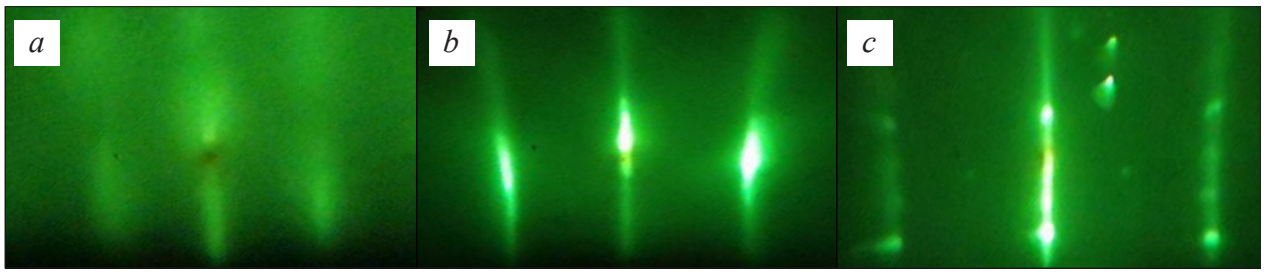

Figure 2. RHEED patterns for $SnSe_2$ growth on (111) Si surface: (*a*) amorphous layer deposition, (*b*) $SnSe_2$ crystallization and growth, (*c*) 3D island formation

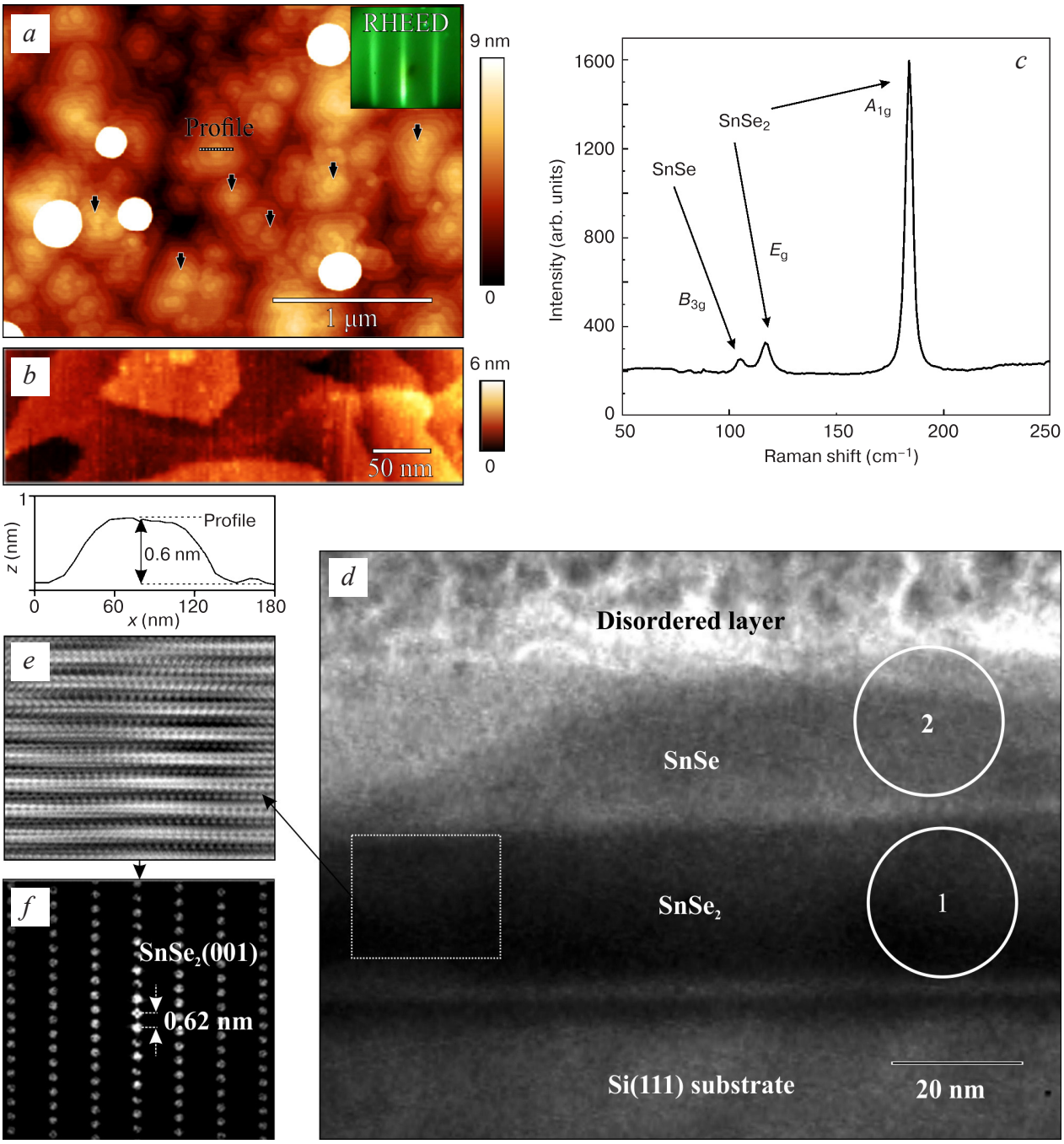

Figure 3. (*a*, *b*) AFM images of $SnSe_2$ film morphology, white areas are 3D SnSe islands, black arrows showing screw-component dislocations, (*c*) Raman spectrum of the film, (*d*) HRTEM image of $SnSe_2$ film cross-section with a 3D SnSe island, (*e*) magnified image of Area 1, (*f*) Fourier image

5. Bi_2Se_3(0001) sublimation during Se deposition

An important difference of Van der Waals substrates from conventional ones is the absence of dangling covalent bonds and hence no necessity of their passivation before growth. Therefore for metal chalcogenide growth on the surface of Van der Waals crystals (e.g. Bi_2Se_3(0001)) the substrate surface is ready for heteroepitaxy immediately after annealing or after cleaving in ultrahigh vacuum, unlike conventional substrates. However, due to the presence of different components (Bi and Se) in the stoichiometric composition, sublimation upon high temperature annealing (>400 °C) occurs anisotropically and non-congruently, i.e., with predominant desorption of selenium from the surface [48]. At the publication time of our earlier works on selenium interaction with silicon surface [25, 27, 34], there was no available literary data on high-temperature Bi_2Se_3 sublimation (>400 °C) with simultaneous selenium deposition onto the surface. On the other hand, the optimum growth temperature of layered metal chalcogenides (e.g. for β-In_2Se_3 it is about 400–450 °C [23, 24]) can be in the range of Bi_2Se_3(0001)

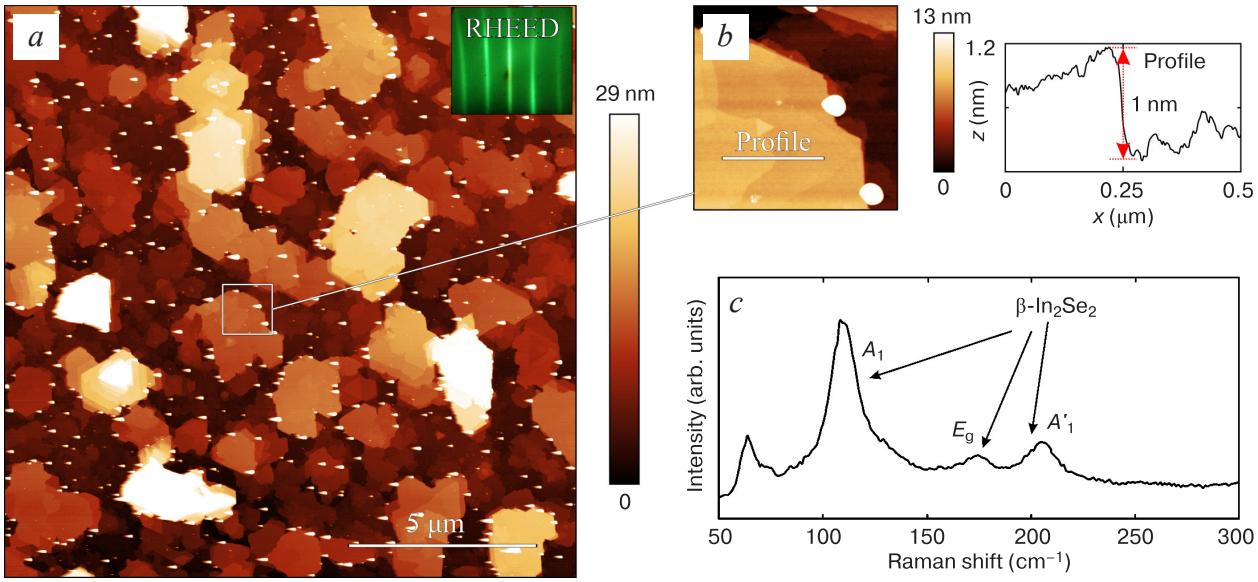

Figure 4. (*a*) AFM image of layered 20 nm thick In_2Se_3 film surface morphology, (*b*) magnified 3D island image and profile across a molecular step, (*c*) Raman spectrum of In_2Se_3 film

substrate sublimation temperatures. Therefore studying Bi_2Se_3 sublimation under preconditions for Van der Waals epitaxy is an important task.

Figure 5(*a*–*c*) shows Bi_2Se_3(0001) surface annealing with simultaneous selenium deposition at a ~0.1 nm/s rate [30]. The REM images show 1 nm high Bi_2Se_3(0001) molecular step flow (dark contrast areas) towards overlaying terraces at about 400 °C at an about 0.02 nm/s velocity [28, 30]. Sublimation of 30 nm (30 Bi_2Se_3 layers) did not lead to changes in terrace contrast and general surface morphology, suggesting congruent sublimation. The AFM surface image (Fig. 5*d*) shows zigzag-shaped steps accounting for the wide dark contrast areas corresponding to molecular steps in the *in situ* REM images. This annealing is used for surface cleaning as a stage of substrate preparation for the growth of layered Van der Waals heterostructures.

The method of synthesizing regular steps on the surface of Van der Waals substrates was first reported [30] which includes the making a lithographic trench on the surface with the hard AFM probe and subsequent annealing at about 400 °C in a selenium flux. Surface sublimation and atomic step ascending flow lead to an increase in the lateral dimensions of the trench (Fig. 5(*e*–*g*)) accompanied by atomic step generation and flow towards overlaying terraces. One can thus increase the concentration of the steps and their average direction relative to the substrate which can be used for surface morphology control aimed at improving the structural perfection of Van der Waals epitaxial layers.

6. Growth of layered Bi_2Se_3, In_2Se_3 and $SnSe_2$ on Bi_2Se_3(0001) surface

Annealing of Bi_2Se_3(0001) surface under congruent sublimation conditions (in a selenium flux) is one of the main stages of substrate surface preparation for further homo- or heteroepitaxial growth. Annealing removes

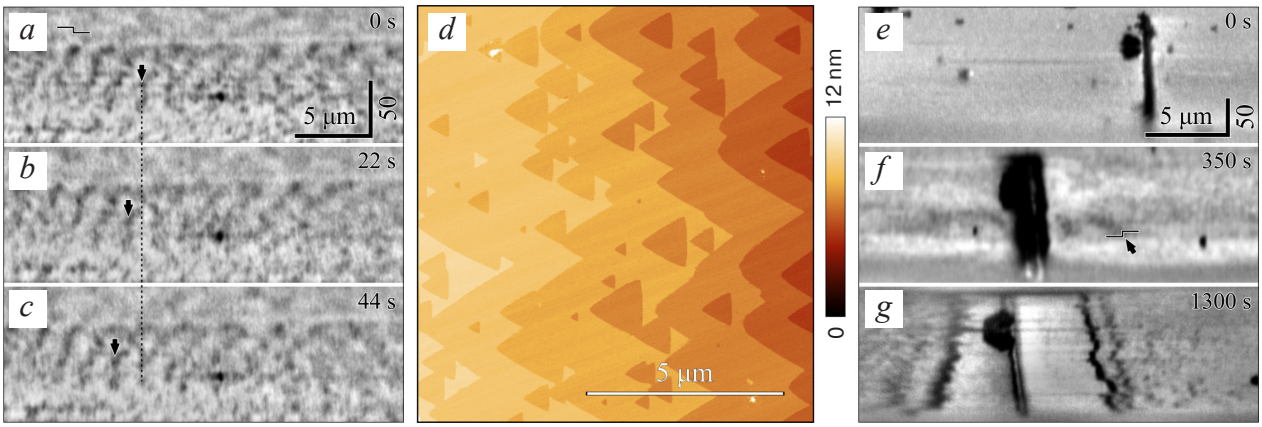

Figure 5. (*a*–*c*) Bi_2Se_3(0001) step flow upper overlaying terraces during congruent sublimation in selenium flux, black arrows show atomic step, (*d*) AFM image of surface morphology after congruent sublimation, (*e*–*g*) synthesis of regular steps by annealing of lithographic trench in selenium flux

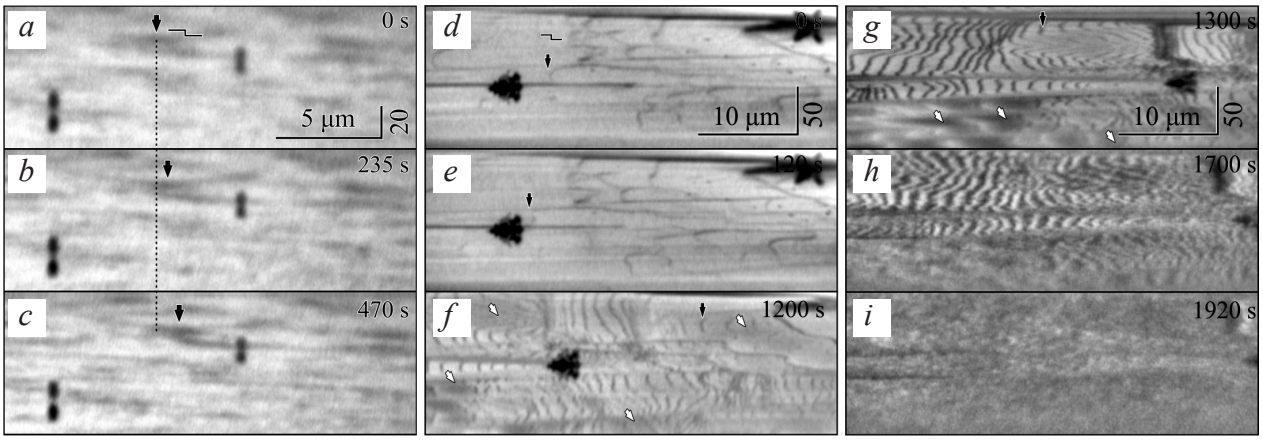

Figure 6. (*a–c*) REM images of homoepitaxial Bi_2Se_3 growth, black arrows show atomic steps; (*d–i*) REM images of indium adsorption for congruent sublimation in selenium flux at 400 °C, black arrows show atomic steps, white arrows show dark contrast areas of terraces due to the precipitation of impurity-induced surface phase islands [28]

atoms adsorbed from the atmosphere and small crystal particles ending up on the surface after specimen cleaving from a single crystal in the atmosphere. If a Bi molecular flux is added to a selenium molecular flux during congruent sublimation at 400 °C, the atomic step flow direction changes to opposite (Fig. 6(*a–c*)), i.e., towards lower terraces, suggesting Van der Waals homoepitaxial growth of Bi_2Se_3(0001). The growth rate in our experiment was about 0.01 nm/s, with no changes being observed in the terrace and step contrast in the REM images and in the RHEED patterns, suggesting Bi_2Se_3(0001) step-flow growth.

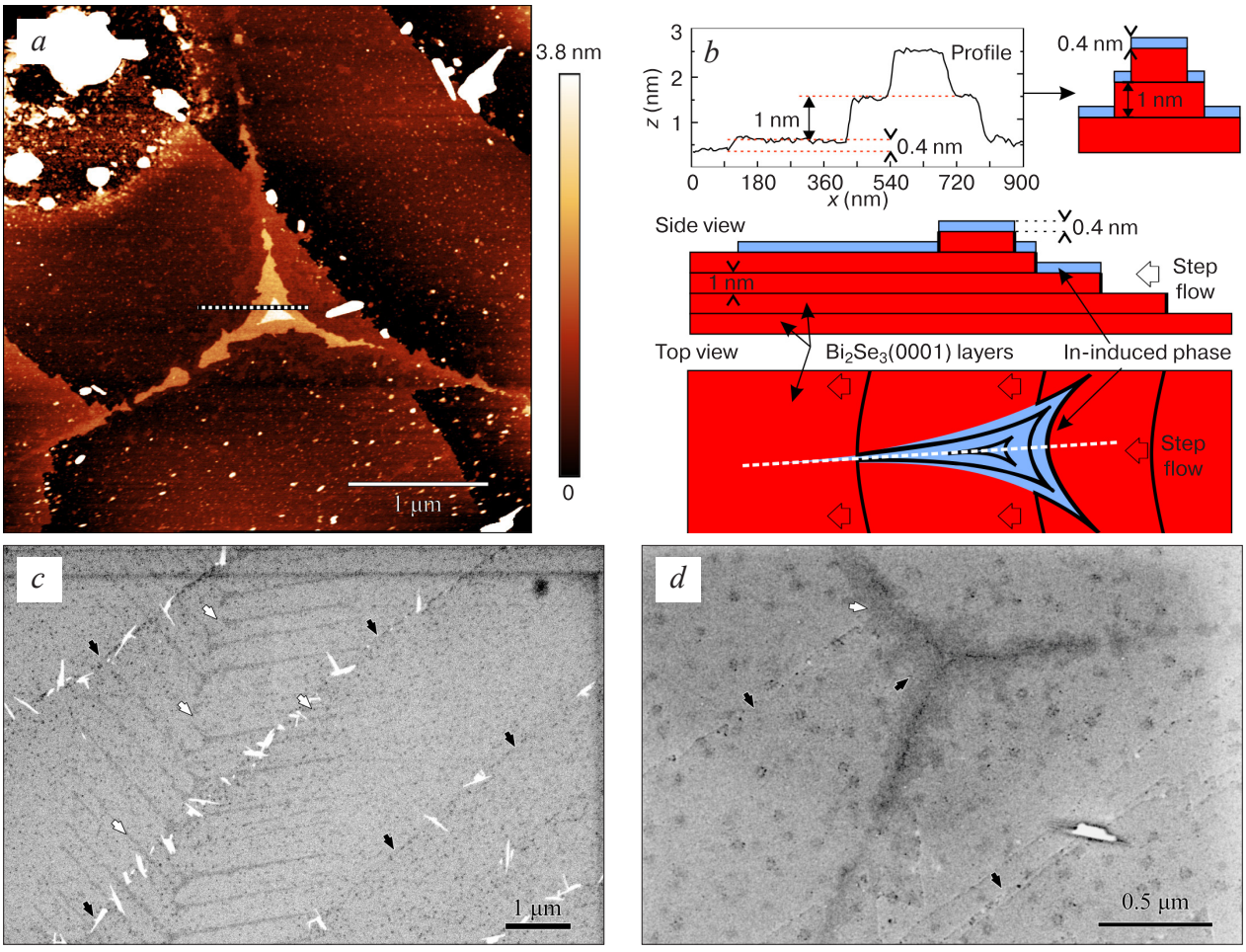

Figure 7. (*a*) AFM image of star-shaped multilayered island formed by local sublimation suppression at 400 °C, (*b*) profile and schematic structure of 2D island formed by impurity-induced indium phase, (*c*, *d*) SEM images of star-shaped islands, black arrows show 1 nm high Bi_2Se_3(0001) atomic steps, white arrows show impurity-induced indium phase

Experiments aimed at studying the Van der Waals heteroepitaxial growth in the *in situ* REM column were carried out under the same conditions as the homoepitaxial growth of Bi_2Se_3 except that an In (or Sn) evaporator was used instead of a Bi one [28]. Indium was deposited at a ~1 nm/h rate simultaneously with a selenium flux. Figure 6(*d*, *e*) shows step flow for congruent surface sublimation at about 400 °C. Then indium was deposited onto the Bi_2Se_3(0001) surface (Fig. 6*d*), causing a broadening of the step contrast (black arrows in Fig. 6(*g*–*i*)). Simultaneously, dark contrast areas formed on the terraces (white arrows in Fig. 6(*g*–*i*)) and covered the terraces from the step edge, indicating the formation of a surface phase which eventually covered the entire Bi_2Se_3(0001) surface.

Ex situ AFM surface morphology study after sub-monolayer indium coating deposition showed the formation of 0.4 nm high impurity-induced surface phase islands on the (0001) Bi_2Se_3 surface which suppress sublimation and eventually form star-shaped multilayered islands which are shown in Fig. 7*a* and schematically in Fig. 7*b*. Figure 7(*c*, *d*) shows backscattered electron SEM surface images sensitive to elemental composition of substrate surface (*Z* contrast indicates higher concentration of greater atomic number atoms corresponding to brighter contrast). White arrows indicate 0.4 nm high star-shaped islands covered with the impurity-induced phase and showing a darker contrast as compared to the rest of the surface, indicating higher indium concentration in the islands.

During further indium deposition in a selenium flux, layered In_2Se_3 starts growing, which produces smooth stripes in the RHEED patterns corresponding to 2D growth. After the In_2Se_3 film thickness reaches 3–5 nm, point reflections emerge in the RHEED patterns that are typical of 3D island growth. *Ex situ* study of the as-grown surface morphology confirmed the formation of a 20 nm thick In_2Se_3 film and 3D islands on the surface (Fig. 8*a*) due to screw-component dislocations emergence (white arrows in Fig. 8*a*). After AFM characterization the specimen phase composition was studied with Raman scattering (Fig. 8*b*) which showed a set of oscillation modes corresponding to β-In_2Se_3 [23, 49] and Bi_2Se_3(0001) [50].

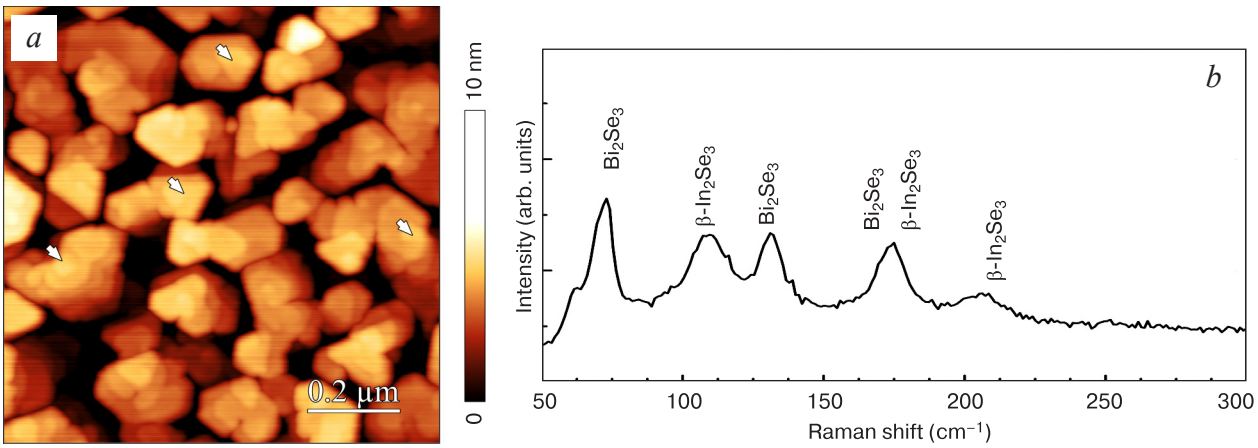

Figure 8. (*a*) AFM images of 20 nm thick In_2Se_3 film surface morphology (islands formed by screw-component dislocations emergence on the surface are marked by white arrows), (*b*) Raman spectrum of In_2Se_3 film on Bi_2Se_3 surface

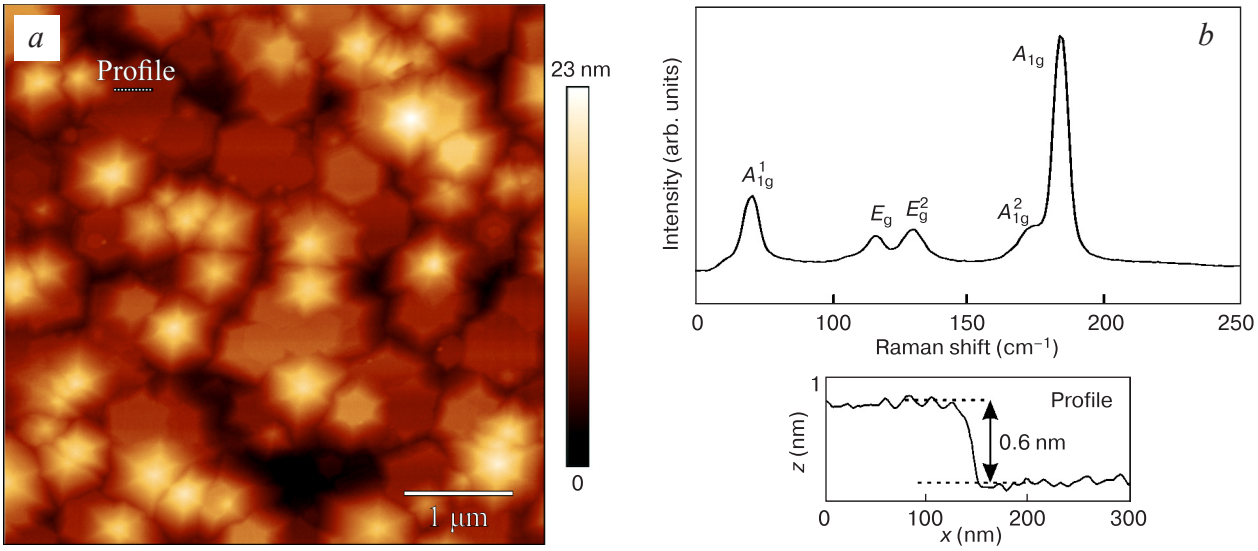

Figure 9. (*a*) AFM image of 30 nm thick $SnSe_2$ film surface morphology, (*b*) Raman spectrum of the as-grown film: oscillation modes E_g and A_{1g} correspond to $SnSe_2$ and $A_{1g}{}^1$, $E_g{}^2$, and $A_{1g}{}^2$, to Bi_2Se_3(0001) substrate

$SnSe_2$ was grown on the $Bi_2Se_3(0001)$ surface using a technique similar to that used for $SnSe_2$ growth on silicon surface, i.e., deposition of a 0.6 nm thick amorphous $SnSe_2$ layer at 100 °C onto the $Bi_2Se_3(0001)$ surface preliminarily annealed in a selenium flux followed by rapid crystallization heating to growth temperatures (200–250 °C). After amorphous layer crystallization the film grew by a multilayered mechanism with gradual attenuation of stripe intensity oscillation amplitude in the RHEED patterns which is typical of 2D island growth, and the emergence of reflections typical of 3D island formation.

The film grown in that experiment had two sets of similarly oriented hexagonal hills covering approximately similar areas of the specimen surface: flat-top and sharp-top ones, formed by screw dislocation emergence on the surface. The flat-top hills that are atomically smooth terraces with lateral dimensions of up to 1 μm did not contain screw dislocations. The AFM images do not show domain boundaries that are typically seen as thin 0.2 nm high lines (example is given in Fig. 3*b*). The low concentration of screw dislocation emergences on the surface and the absence of domain boundaries in the AFM images indicate low concentration of structural defects in the film and evidence the epitaxial growth of films. Hills of the other type (pyramid-shaped) are typical of grown metal chalcogenide films [12, 43] and occupy the other half of the surface area, the surface-average concentration of screw dislocation emergences being ~2 μm^{-2} which is almost by one order of magnitude lower than for $SnSe_2$ growth on silicon surface and in comparison with earlier data, i.e., ~32 μm^{-2} [43] and ~30 μm^{-2} [51]. Thus, annealing of the $Bi_2Se_3(0001)$ substrate in a selenium flux and amorphous metal chalcogenide layer crystallization significantly reduce the concentration of screw defects and hence improve the structural perfection of the growing films.

7. Conclusion

The capabilities of the unique *in situ* REM method at studying processes on the surfaces of Van der Waals and conventional semiconductor substrates have been demonstrated on the examples of Si(111) and $Bi_2Se_3(0001)$ surfaces. A series of *in situ* REM studies coupled with complementary *ex situ* AFM, Raman scattering, SEM and HRTEM methods delivered new information on atomic processes on the Si(111) and $Bi_2Se_3(0001)$ surfaces occurring during the sublimation and growth of layered metal chalcogenides, e.g. the effect of Si(111) surface passivation on the orientation of 2D layered metal chalcogenide islands forming during the growth, a technique of reducing defect concentration in the growing films by amorphous layer crystallization and interaction of indium atoms with Bi_2Se_3 surface. The data obtained in this work help developing practical surface structure and morphology control tools for further growth of heterostructures using Van der Waals epitaxy techniques.

Physical laws of interaction between a selenium molecular beam and Si(111) and $Bi_2Se_3(0001)$ surfaces were studied using the *in situ* REM, a structural kinetic diagram of selenium interaction with Si(111) surface at 600–1350 °C was obtained and high-temperature $Bi_2Se_3(0001)$ sublimation was demonstrated for conditions when intense selenium desorption from the surface is compensated by a selenium molecular beam. Indium adsorption onto $Bi_2Se_3(0001)$ surface was found to be accompanied by the formation of 0.4 nm high impurity-induced phase 2D islands which locally suppress sublimation. Homo- and heteroepitaxial metal chalcogenide film (Bi_2Se_3, $SnSe_2$ and In_2Se_3) growth techniques were developed that provide low defect concentration on Si(111) and $Bi_2Se_3(0001)$ surfaces and include an amorphous layer crystallization stage. $SnSe_2$ epitaxial films were grown with low concentrations of screw dislocation emergence on the surface, i.e., ~2 μm^{-2} on a $Bi_2Se_3(0001)$ substrate and ~18 μm^{-2} on a passivated Si(111) surface. For a $SnSe_2$ film on $Bi_2Se_3(0001)$ surface, dislocation-free hills were first observed the top terraces of which were ~1 μm in size. The data presented in this work establish a basis for further *in situ* studies of early growth stages of layered metal chalcogenides, Van der Waals epitaxy of other metal chalcogenides and multilayered heterostructures for solving Van der Waals epitaxy issues.

Acknowledgments

$SnSe_2$ growth on Si(111) surface was carried out with support from State Assignment (Project No. FWGW-2022-0007). Indium adsorption and $SnSe_2$ growth on $Bi_2Se_3(0001)$ surface were conducted with support from the Russian Science Foundation (Grant No. 22-72-10124). Studies of selenium beam interaction with Si(111) surface were carried out with support from the Russian Science Foundation (Grant No. 18-72-10063). Sublimation and Bi_2Se_3 growth were conducted with support from the Russian Science Foundation (Grant No. 19-72-30023).

References

1. Geim A.K., Novoselov K.S. The rise of graphene. *Nature Materials.* 2007; 6(3): 183–191. https://doi.org/10.1038/nmat1849
2. Novoselov K.S., Jiang D., Schedin F., Booth T.J., Chotkevich V.V., Morozov S.V., Geim A.K. Two-dimensional atomic crystals. *Proceedings of the National Academy of Sciences.* 2005; 102(30): 10451–10453. https://doi.org/10.1073/pnas.0502848102
3. Geim A.K., Grigorieva I.V. Van der Waals heterostructures. *Nature.* 2013; 499(7459): 419–425. https://doi.org/10.1038/nature12385

4. Zhang K., Zhang T., You J., Zheng X., Zhao M., Zhang L., Kong J., Luo Z., Huang S. Low-temperature vapor-phase growth of 2D metal chalcogenides. *Small.* 2024; 20(19): 2307587. https://doi.org/10.1002/smll.202307587
5. Giri A., Park G., Jeong U. Layer-structured anisotropic metal chalcogenides: recent advances in synthesis, modulation, and applications. *Chemical Reviews.* 2023; 123(7): 3329–3442. https://doi.org/10.1021/acs.chemrev.2c00455
6. Lu Z., Neupane G.P., Jia G., Zhao H., Qi D., Du Y., Lu Y., Yin Z. 2D materials based on main group element compounds: phases, synthesis, characterization, and applications. *Advanced Functional Materials*. 2020; 30(40): 2001127. https://doi.org/10.1002/adfm.202001127
7. Zibouche N., Philipsen P., Kuc A., Heine T., Transition-metal dichalcogenide bilayers: switching materials for spintronic and valleytronic applications. *Physical Review B.* 2014; 90(12): 125440. https://doi.org/10.1103/PhysRevB.90.125440
8. Vishwanath S., Liu X., Rouvimov S., Basile L., Lu N., Azcatl A., Magno K., Wallace R.M., Kim M., Idrobo J.-C., Furdyna J.K., Jena D., Xing H.G. Controllable growth of layered selenide and telluride heterostructures and superlattices using molecular beam epitaxy. *Journal of Materials Research.* 2016; 31(7): 900–910. https://doi.org/10.1557/jmr.2015.374
9. Chen M.M., Xue H.G., Guo S.-P. Multinary metal chalcogenides with tetrahedral structures for second-order nonlinear optical, photocatalytic, and photovoltaic applications. *Coordination Chemistry Reviews*. 2018; 368: 115–133. https://doi.org/10.1016/j.ccr.2018.04.014
10. Gao M.R., Xu Y.F., Jiang J., Yu S.-H. Nanostructured metal chalcogenides: synthesis, modification, and applications in energy conversion and storage devices. *Chemical Society Reviews*. 2013; 42(7): 2986–3017. https://doi.org/10.1039/c2cs35310e
11. Buffiere M., Dhawale D.S., El Mellouhi F. Chalcogenide materials and derivatives for photovoltaic applications. *Energy Technology*. 2019; 7(11): 1900819. https://doi.org/10.1002/ente.201900819
12. Claro M., Grzonka J., Nicoara N., Ferreira P., Sadewasser S. Wafer-scale fabrication of 2D β-In_2Se_3 photodetectors. *Advanced Optical Materials.* 2020; 9: 2001034. https://doi.org/10.1002/adom.202001034
13. Wang F., Zhang Y., Gao Y., Luo P., Su J., Han W., Liu K., Li H., Zhai T. 2D metal chalcogenides for IR photodetection. *Small.* 2019; 15(30): e1901347. https://doi.org/10.1002/smll.201901347
14. Yang Z., Hao J. Recent progress in 2D layered III–VI semiconductors and their heterostructures for optoelectronic device applications. *Advanced Materials Technologies.* 2019; 4(8): 1900108. https://doi.org/10.1002/admt.201900108
15. Li J., Li H., Niu X., Wang Z. Low-dimensional In_2Se_3 compounds: from material preparations to device applications. *ACS Nano.* 2021; 15(12): 18683–18707. https://doi.org/10.1021/acsnano.1c03836
16. Late D.J., Huang Y.K., Liu B., Acharya J., Shirodkar S.N., Luo J., Yan A., Charles D., Waghmare U.V., Dravid V.P., Rao C.N. Sensing behavior of atomically thin-layered MoS_2 transistors. *ACS Nano.* 2013; 7(6): 4879–4891. https://doi.org/10.1021/nn400026u
17. Li H., Yin Z., He Q., Li H., Huang X., Lu G., Fam D.W., Tok A.Y., Zhang Q., Zhang H. Fabrication of single- and multilayer MoS_2 film-based field-effect transistors for sensing NO at room temperature. *Small.* 2012; 8(1): 63–67. https://doi.org/10.1002/smll.201101016
18. Liao W., Huang Y., Wang H., Zhang H., Van der Waals heterostructures for optoelectronics: progress and prospects. *Applied Materials Today*. 2019; 16: 435–455. https://doi.org/10.1016/j.apmt.2019.07.004
19. Bao X., Ou Q., Xu Z.-Q., Zhang Y., Bao Q., Zhang H. Band structure engineering in 2D materials for optoelectronic applications. *Advanced Materials Technologies*. 2018; 3(11): 1800072. https://doi.org/10.1002/admt.201800072
20. Lasek K., Coelho M.C., Zberecki K., Xin Y., Kolekar S.K., Li J., Batzill M. Molecular beam epitaxy of transition metal (Ti-, V-, and Cr-) tellurides: from monolayer ditellurides to multilayer self-intercalation compounds. *ACS Nano.* 2020; 14(7): 8473–8484. https://doi.org/10.1021/acsnano.0c02712
21. Callaert C., Bercs M., Lamoen D., Hadermann J. Interstitial defects in the Van der Waals gap of Bi_2Se_3. *Acta Crystallographica Section B: Structural Science, Crystal Engineering and Materials*. 2019; 75(Pt 4): 717–732. https://doi.org/10.1107/S2052520619008357
22. Kampmeier J., Borisova S., Plucinski L., Luysberg M., Mussler G., Grutzmacher D. Suppressing twin domains in molecular beam epitaxy grown Bi_2Te_3 topological insulator thin films. *Crystal Growth & Design*. 2015; 15(1): 390–394. https://doi.org/10.1021/cg501471z
23. Liu L., Dong J., Huang J., Nie A., Zhai K., Xiang J., Wang B., Wen F., Mu C., Zhao Z., Gong Y., Tian Y., Liu Z. Atomically resolving polymorphs and crystal structures of In_2Se_3. *Chemistry of Materials.* 2019; 31(24): 10143–10149. https://doi.org/10.1021/acs.chemmater.9b03499
24. Li S., Yan Y., Deng Q., Yu Z., Zhang Y., Jiang Y., Song X., Zhao H., Su J., Li J., Xia C. Substrate-induced phase control of In_2Se_3 thin films. *Journal of Alloys and Compounds.* 2020; 845: 156270. https://doi.org/10.1016/j.jallcom.2020.156270
25. Rogilo D.I., Sitnikov S.V., Rodyakina E.E., Petrov A.S., Ponomarev S.A., Shcheglov D.V., Fedina L., Latyshev A. *In situ* reflection electron microscopy for the analysis of silicon surface processes: sublimation, electromigration, and adsorption of impurity atoms. *Crystallography Reports.* 2021; 66(4): 570–580. https://doi.org/10.1134/S1063774521040192
26. Ponomarev S.A., Rogilo D.I., Petrov A.S., Sheglov D.V., Latyshev A.V. Etching kinetics of Si(111) surface by selenium molecular beam. *Optoelectronics Instrumentation and Data Processing.* 2020; 56(5): 449–455. https://doi.org/10.3103/S8756699020050088
27. Rogilo D.I., Sitnikov S.V., Ponomarev S.A., Sheglov D.V., Fedina L.I., Latyshev A.V. Structural and morphological instabilities of the Si(111)-7×7 surface during silicon growth and etching by oxygen and selenium. *Applied Surface Science*. 2021; 540(114): 148269. https://doi.org/10.1016/j.apsusc.2020.148269
28. Ponomarev S.A., Rogilo D.I., Nasimov D.A., Kokh K.A., Sheglov D.V., Latyshev A.V. High-temperature indium adsorption on Bi_2Se_3(0001) surface studied by *in situ* reflection electron microscopy. *Journal of Crystal Growth.* 2024; 628: 127545. https://doi.org/10.1016/j.jcrysgro.2023.127545
29. Ponomarev S.A., Zakhozhev K.E., Rogilo D.I., Gutakovsky A.K., Kurus N.N., Kokh K.A., Sheglov D.V., Milekhin A.G., Latyshev D.V. Low-defect-density $SnSe_2$ films nucleated via thin layer crystallization. *Journal of Crystal Growth*. 2024; 631: 127615. https://doi.org/10.1016/j.jcrysgro.2024.127615
30. Ponomarev S.A., Rogilo D.I., Kurus N.N., Basalaeva L.S., Kokh K.A., Milekhin A.G., Sheglov D.V., Latyshev A.V. *In situ* re-

flection electron microscopy for investigation of surface processes on Bi_2Se_3(0001). *Journal of Physics Conference Series*. 2021; 1984(1): 012016. https://doi.org/10.1088/1742-6596/1984/1/012016

31. Latyshev A.V., Fedina L.I., Rogilo D.I., Sitnikov S.V., Kosolobov S.S. Atomically controlled silicon surface. Novosibirsk: Parallel; 2016. 220 p.
32. Nobuyuki O., Tanishiro Y., Yagi K., Honjo G. Image contrast of dislocations and atomic steps on (111) silicon surface in reflection electron microscopy. *Surface Science.* 1981; 102(2-3): 424–442. https://doi.org/10.1016/0039-6028(81)90038-8
33. Ponomarev S.A., Zakhozhev K.E., Rogilo D.I., Kurus N.N., Sheglov D.V., Milekhin A.G., Latyshev A.V. Ponomarev S.A., Zakhozhev K.E., Rogilo D.I., Kurus N.N., Sheglov D.V., Milekhin A.G., Latyshev A.V. Van der Waals heteroepitaxial growth of layered $SnSe_2$ on surfaces Si(111) and Bi_2Se_3. *Optoelectronics, Instrumentation and Data Processing.* 2022; 58(6): 564–570. https://doi.org/10.3103/S8756699022060097
34. Rogilo D.I., Fedina L.I., Ponomarev S.A., Sheglov D.V., Latyshev A.V. Etching of step-bunched Si(111) surface by Se molecular beam observed by *in situ* REM. *Journal of Crystal Growth.* 2020; 529: 125273. https://doi.org/10.1016/j.jcrysgro.2019.125273
35. Petrov A.S., Rogilo D.I., Zhachuk R.A., Vergules A.I., Sheglov D.V., Latyshev A.V. Structural transitions on Si(111) surface during Sn adsorption, electromigration, and desorption studied by *in situ* UHV REM. *Applied Surface Science*. 2023; 609: 155367. https://doi.org/10.1016/j.apsusc.2022.55367
36. Papageorgopoulos A.C., Kamaratos M. A Study of the restoration of Se/Si(111)-7×7 reconstructed surfaces: Preservation of the bulk-terminated state. *Surface Science.* 2002; 504(1-3): 191–195. https://doi.org/10.1016/S0039-6028(02)01096-8
37. Tao M., Udeshi D., Basit N., Maldonado E., Kirk W.P. Removal of dangling bonds and surface states on silicon (001) with a monolayer of selenium. *Applied Physics Letters.* 2003; 82(10): 1559–1561. https://doi.org/10.1063/1.1559418
38. Dev B.N., Thundat T., Gibson W.M. An X-ray standing wave interference spectrometric analysis of chemisorption of selenium on silicon (111) and (220) surfaces. *Journal of Vacuum Science & Technology A: Vacuum, Surfaces, and Films.* 1985; 3(3): 946–949. https://doi.org/10.1116/1.573357
39. Wu S.Q., Zhou Y., Wu Q.H., Pakes C.I., Zhu Z.Z. Adsorption of selenium atoms at the Si(111)-7×7 surface: A combination of scanning tunnelling microscopy and density functional theory studies. *Chemical Physics*. 2011; 382(1-3): 41–46. https://doi.org/10.1016/j.chemphys.2011.02.006
40. Takayanagi K., Tanishiro Y., Takahashi S., Takahashi M. Structure analysis of Si(111)-7×7 reconstructed surface by transmission electron diffraction. *Surface Science.* 1985; 164: 367–392. https://doi.org/10.1016/0039-6028(85)90753-8
41. Aretouli K.E., Tsoutsou D., Tsipas P., Velasco J.M., Giamini S.A., Kelaidis N., Psycharis V., Dimoulas A. Epitaxial 2D $SnSe_2$/2D WSe_2 Van der Waals heterostructures. *ACS Applied Materials & Interfaces.* 2016; 8(35): 23222–23229. https://doi.org/10.1021/acsami.6b02933
42. Thomas B. Effect of *in situ* post-deposition annealing on the formation of α-In_2Se_3 thin films grown by elemental evaporation. *Applied Physics A: Solids Surfaces*. 1992; 54(3): 293–299. https://doi.org/10.1007/BF00323853
43. Matetskiy A.V., Kibirev I.A., Zotov A.V., Saranin A.A. Growth and characterization of Van der Waals heterostuctures formed by the topological insulator Bi_2Se_3 and the trivial insulator $SnSe_2$. *Applied Physics Letters.* 2016; 109(2): 021606. https://doi.org/10.1063/1.4958936
44. Wu J., Hu Z., Jin Z., Lei S., Guo H., Chatterjee K., Zhang J., Yang Y., Li B., Liu Y., Lai J., Vajtai R., Yakobson B., Tang M., Lou J., Ajayan P.M. Spiral growth of $SnSe_2$ crystals by chemical vapor deposition. *Advanced Materials Interfaces.* 2016; 3(16): 1600383. https://doi.org/10.1002/admi.201600383
45. Liu F., Parajuli P., Rao R., Wei P.-C., Karunarathne A., Bhattacharya S., Podila R., He J., Maryama B., Priyadarshan G., Gladden J.R., Chen Y.Y., Rao A.M. Phonon anharmonicity in single-crystalline SnSe. *Physical Review B.* 2018; 98(22): 224309. https://doi.org/10.1103/PhysRevB.98.224309
46. Balakrishnan N., Staddon C.R., Smith E.F., Stec E.F., Gay J., Mudd G.W., Makarovsky O., Kurdtynskyi Z.R., Kovalyuk Z.D., Eaves L., Patane A., Beton P.H. Quantum confinement and photoresponsivity of β-In_2Se_3 nanosheets grown by physical vapour transport. *2D Materials*. 2016; 3(2): 025030. https://doi.org/10.1088/2053-1583/3/2/025030
47. Ponomarev S., Rogilo D., Mironov A., Sheglov D., Latyshev A. Thermal hysteresis in the resistance of In_2Se_3 film on Si(111) surface. In: *2021 IEEE 22nd Int. conf. young prof. electron devices materials (EDM). Souzga, the Altai Republic, Russia*. IEEE; 2021. P. 50–53. https://doi.org/10.1109/EDM52169.2021.9507592
48. Buha J., Gaspari R., Sastillo A., Bonaccorso F., Manna L. Thermal stability and anisotropic sublimation of two-dimensional colloidal Bi_2Te_3 and Bi_2Se_3 nanocrystals. *Nano Letters*. 2016; 16(7): 4217–4223. https://doi.org/10.1021/acs.nanolett.6b01116
49. Tao X., Gu Y. Crystalline-crystalline phase transformation in two-dimensional In_2Se_3 thin layers. *Nano Letters.* 2013; 13(8): 3501–3505. https://doi.org/10.1021/nl400888p
50. Zhang J., Peng Z., Soni A., Zhao Y., Xiong Y., Peng B., Wang J., Dresselhaus M.S., Xiong Q. Raman spectroscopy of few-quintuple layer topological insulator Bi_2Se_3 nanoplatelets. *Nano Letters*. 2011; 11(6): 2407–2414. https://doi.org/10.1021/nl200773n
51. Wang C., Yang H., Wang Q., Qiao L., Peng X., Li J., Han J., Wang Q., Li X., Wang Z., Duan J., Xiao W. Controllable growth of two-dimensional $SnSe_2$ flakes with screw dislocations and fractal structures. *CrystEngComm.* 2020; 22(32): 5296–5301. https://doi.org/10.1039/D0CE00819B